Fibre Path Planning for Automated Fibre Placement on Doubly Curved Structures

Avyadhish Malladi*, Christos Kassapoglou*, Daniël Peeters*
*Faculty of Aerospace Engineering, Delft University of Technology,
Kluyverweg 1, 2629 HS Delft, The Netherlands

ABSTRACT

Variable-stiffness laminates, enabled by automated fibre placement, offer improved structural performance through spatially varying fibre orientations. A three-step design framework comprising stiffness optimisation, fibre angle retrieval, and fibre path generation has been developed to realise such laminates, of which fibre path generation is the subject of this work. Doubly curved geometries with Gaussian curvature are predominant in aerospace structures, yet extracting streamline-based courses at prescribed spacing on such surfaces remains insufficiently addressed in the literature. This paper proposes a geodesic course extraction method that guarantees overlap-free placement on curved surfaces, with gaps tolerated as a design concession, demonstrated on a doubly curved geometry.

1. Introduction

Conventional fibre-reinforced composite laminates are typically designed by stacking plies with discrete fibre orientations of 0°, ±45°, and 90°. This conservative approach has long been favoured by industry owing to decades of accumulated experience, producing a wealth of data establishing allowable values for such designs. However, the absence of equivalent data for non-conventional configurations and the lack of an efficient low-cost certification approach have hindered the industry's transition away from standard layups. Research suggests that spatially varying in-plane fibre orientations introduce a continuous stiffness variation across the laminate, facilitating more effective load redistribution and improved structural performance [2]. Advances in automated fibre placement (AFP) technology have made it feasible to steer fibres at scale, enabling the realisation of variable stiffness laminates (VSL) [8]. The principal challenge therefore shifts to the design domain.

A three-step design framework has been developed at the Delft University of Technology [4] (see Figure 1). In the first step, lamination parameters are used to spatially optimise the stiffness distribution across the target geometry. In the second step, a fibre angle retrieval operation recovers the local orientations that represent the designed stiffness distribution. Finally, these fibre angle distributions are converted into continuous fibre paths that an AFP robot head can follow. The final is the focus of the present work.

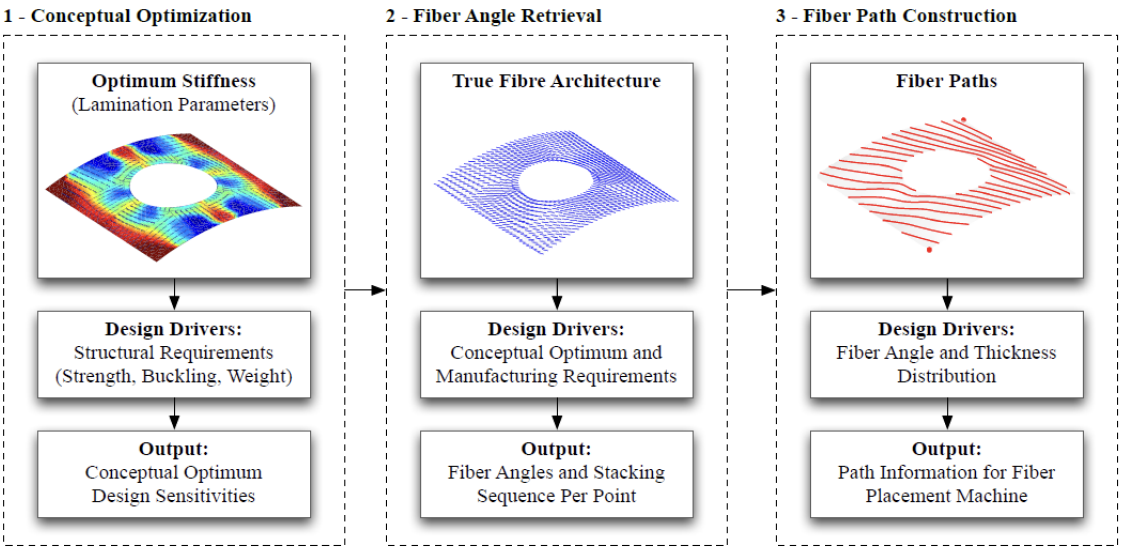

Figure 1: Overview of the three-step process for VSL design [4]

In the literature, several methods have been proposed to translate fibre angle distributions into AFP-compatible towpaths. Blom et al. established the Streamline Analogy, treating the fibre angle distribution as a vector field and representing tow-paths as streamlines, demonstrating good results for 2D geometries [1]. Hijne proposed a progenitor-offset method with manufacturability-driven angle discretisation into constant and continuously varying regions, though it is limited to linearly varying fibre angle distributions [3]. Peeters et al. developed the FIPAM tool, assembling initial paths from kriging-interpolated segments subsequently fitted with Bézier curves to enforce manufacturing constraints [6]. Lozano et al. later applied this to plates with cut-outs and fairings, though constant fibre angles were used in the latter case [5]. Pupo et al. proposed a 3D-to-2D mapping strategy to leverage existing 2D techniques for 3D structures, though this faces fundamental limitations for non-developable geometries [7]. This is because non-developable surfaces cannot be flattened without distortion, meaning courses planned at uniform spacing in 2D will exhibit gaps or overlaps when deposited on the actual curved surface.

The Streamline Analogy is rooted in fluid dynamics and can extend naturally from planar to three-dimensional geometries. The resulting streamlines closely conform to the prescribed fibre angle distribution while remaining continuous. Although previously applied to a two-dimensional case [1], its extension to doubly-curved surfaces typical of aircraft structural components remains largely unexplored. On planar geometries, streamlines can be extracted directly at the prescribed inter-tow spacing. On doubly-curved surfaces, however, uniform spacing can no longer be trivially enforced, and this challenge is something that needs to be addressed when extending the streamline analogy to doubly-curved surfaces. This paper utilises the Streamline Analogy to obtain fibre paths on a doubly-curved geometry and proposes a course extraction approach to obtain tows at prescribed inter-tow spacing. The methodology is described in Section 2, followed by the results in Section 3. Finally, the conclusions are drawn in Section 4.

2. Streamline Algorithm

The Streamline Algorithm (SA) converts optimised fibre angle distributions into manufacturable tow-paths for AFP. Drawing inspiration from fluid dynamics, the approach treats fibre orientations across the surface as a vector field, with tow-paths emerging as streamlines of that field. To achieve this, smooth local reference frames are first constructed across the surface. Inflow and outflow boundaries are then identified, and a thickness distribution is computed to model how material accumulates as tows traverse the surface; this weighted field serves as the source for a stream function whose iso-contours represent candidate fibre trajectories. Course centrelines are finally extracted at spacings that satisfy AFP manufacturing constraints. Throughout this paper, the algorithm is illustrated using a simple Gaussian-curvature geometry (Figure 2) as a running example. A synthetic fibre angle distribution is prescribed at each mesh node using equation 1, superimposing linear, radial, and sinusoidal components to produce a smooth yet spatially varying field.

$$\theta_i = 30 + 25\hat{x}_i + 7\hat{\rho}_i + 4\sin(3\pi\,(\hat{y}_i + 0.5)) \tag{1}$$

where $\hat{x}_i$ and $\hat{y}_i$ are the normalised planar coordinates of node i, and $\hat{\rho}_i = \rho_i/\rho_{\max}$ is the normalised radial distance from a prescribed focal point, set here to the midpoint of the nodal $\hat{x}_i$ and $\hat{y}_i$ coordinate ranges. The sinusoidal term introduces spatially varying angular modulation into the fibre angle distribution. This distribution is deliberately chosen to exercise the full generality of the algorithm, as purely linear or uniform angle fields would trivially reduce to parallel tow-paths and fail to reveal the geometric complexity the method is designed to handle. The resulting distribution is illustrated in Figure 3.

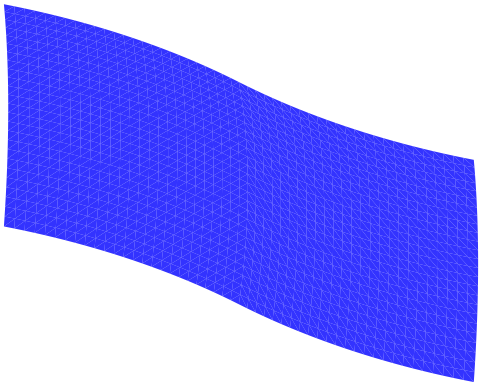

Figure 2: Gaussian-curvature geometry

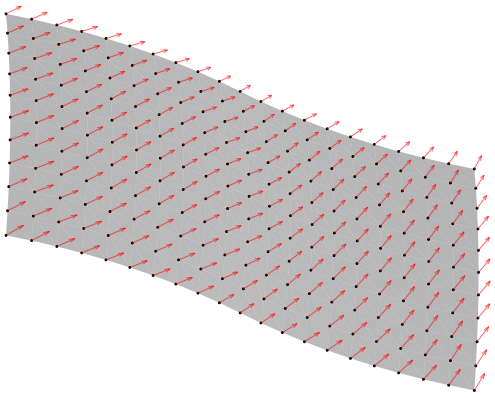

Figure 3: Fibre angle distribution

2.1. Reference Frame Assignment

Local reference frames are constructed at each node by first selecting a temporary vector $\boldsymbol{p}_{\text{temp}}$ aligned with the coordinate axis where, the unit normal $\boldsymbol{N}_i$ at node i, exhibits the smallest absolute component. This choice maximises the angular separation between $\boldsymbol{p}_{\text{temp}}$ and $\boldsymbol{N}_i$, ensuring the subsequent tangent-plane projection (Equation 2) is well-conditioned

and avoids a near-parallel degeneracy. The orthogonal direction is then obtained via $\boldsymbol{q}_i = \boldsymbol{N}_i \times \boldsymbol{p}_i$.

$$\boldsymbol{p}_i = \frac{\boldsymbol{p}_{\text{temp}} - (\boldsymbol{p}_{\text{temp}} \cdot \boldsymbol{N}_i)\boldsymbol{N}_i}{\|\boldsymbol{p}_{\text{temp}} - (\boldsymbol{p}_{\text{temp}} \cdot \boldsymbol{N}_i)\boldsymbol{N}_i\|} \tag{2}$$

While these initial frames satisfy local orthogonality, they may exhibit discontinuous orientations across element boundaries. To ensure smooth spatial variation, an energy functional (Equation 3) penalising sharp orientation variations between adjacent elements is minimised.

$$G = \sum_e \frac{s_u^2 + s_v^2}{8A_e} \quad \text{where} \quad s_u = \sum_{i=1}^{3} \boldsymbol{l}_i \cdot \boldsymbol{p}_i, \quad s_v = \sum_{i=1}^{3} \boldsymbol{l}_i \cdot \boldsymbol{q}_i \tag{3}$$

Here, $\boldsymbol{l}_i$ denotes element edge vectors and A_e represents element area. Correction angles $\boldsymbol{\phi}$ are obtained by solving $\boldsymbol{L}\boldsymbol{\phi} = \boldsymbol{g}$, where $\boldsymbol{L}$ is the Laplacian matrix (assembled as $L_{ij} = \sum_e \boldsymbol{l}_i \cdot \boldsymbol{l}_j/(4A_e)$) and $\boldsymbol{g} = -\partial G/\partial \boldsymbol{\phi}$ is the energy gradient. The descent direction $\delta = \boldsymbol{g}^T\boldsymbol{\phi}$ quantifies the expected energy reduction.

An adaptive approach controls rotation magnitude through a scaling parameter α, which is increased when the energy decreases and reduced otherwise, ensuring stable convergence. Reference frames are iteratively updated according to:

$$\boldsymbol{p}' = \boldsymbol{p}\cos(\phi/\alpha) + \boldsymbol{q}\sin(\phi/\alpha), \quad \boldsymbol{q}' = -\boldsymbol{p}\sin(\phi/\alpha) + \boldsymbol{q}\cos(\phi/\alpha) \tag{4}$$

The updated energy G_n is evaluated and an adaptive step size controls the update magnitude. Convergence is declared when $\max|\phi| < 10^{-5}$ or $(G - G_n)/G < 10^{-5}$. The converged smooth reference frames are aligned with a prescribed global reference direction $\boldsymbol{p}_{\text{ref}}$ through a uniform rotation. The alignment angle is determined by area-weighted projection:

$$\theta_0 = \arctan(S_q/S_p) \quad \text{where} \quad S_p = \sum_i (\boldsymbol{p}_i \cdot \boldsymbol{p}_{\text{ref}})A_{e,i}, \quad S_q = \sum_i (\boldsymbol{q}_i \cdot \boldsymbol{p}_{\text{ref}})A_{e,i} \tag{5}$$

Applying this rotation yields the intrinsic manufacturing reference frames:

$$\boldsymbol{p}_{m,i} = \boldsymbol{p}_i' \cos(\theta_0) + \boldsymbol{q}_i' \sin(\theta_0), \quad \boldsymbol{q}_{m,i} = -\boldsymbol{p}_i' \sin(\theta_0) + \boldsymbol{q}_i' \cos(\theta_0) \tag{6}$$

These manufacturing frames are subsequently rotated by the prescribed fibre angles θ_i at each node to yield the fibre-aligned frames used for streamline generation:

$$\tilde{\boldsymbol{p}}_i = \boldsymbol{p}_{m,i}\cos(\theta_i) + \boldsymbol{q}_{m,i}\sin(\theta_i), \quad \tilde{\boldsymbol{q}}_i = -\boldsymbol{p}_{m,i}\sin(\theta_i) + \boldsymbol{q}_{m,i}\cos(\theta_i) \tag{7}$$

The resultant reference frames are shown in Figure 4.

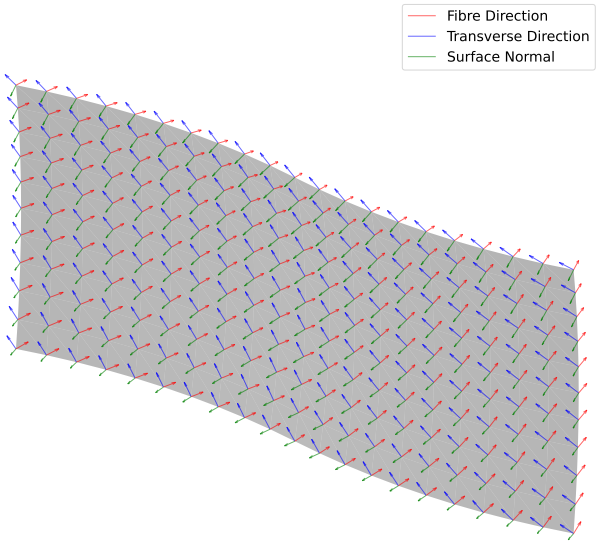

Figure 4: Reference frames resulting from the given fibre angle distribution

2.2. Thickness Distribution

Inflow and outflow boundaries are identified by evaluating the alignment between boundary edge normals and fibre orientations. The thickness distribution quantifies material accumulation as continuous fibre tows, following prescribed orientations, pass from inflow nodes through the surface to outflow boundaries. The objective is to compute an optimal distribution that minimises total material volume whilst ensuring smooth thickness variation in the direction transverse to the fibres. Abrupt thickness changes produce surface unevenness detrimental to both bonding quality and aerodynamic performance.

To achieve smooth thickness variation, the problem is formulated as an energy minimisation that penalises rapid thickness changes transverse to fibre directions:

$$E = \frac{1}{2}\boldsymbol{h}^T\boldsymbol{K}\boldsymbol{h} \quad \text{where} \quad K_{ij}^{(e)} = \frac{(\boldsymbol{l}_i \cdot \tilde{\boldsymbol{q}}_i)(\boldsymbol{l}_j \cdot \tilde{\boldsymbol{q}}_j)}{4A_e} \tag{8}$$

where $\boldsymbol{l}_i$ denotes element edge vectors, $\tilde{\boldsymbol{q}}_i$ the fibre-aligned transverse direction at node i (from Equation 7), and A_e the element area.

Since material enters only at inflow nodes, the thickness field is fully determined by the inflow boundary conditions. Partitioning nodes as $\boldsymbol{h} = [\boldsymbol{h}_{\text{oth}}, \boldsymbol{h}_{\text{in}}]^T$ and the stiffness matrix accordingly:

$$\boldsymbol{K} = \begin{bmatrix} \boldsymbol{K}_{\text{oo}} & \boldsymbol{K}_{\text{oi}} \\ \boldsymbol{K}_{\text{io}} & \boldsymbol{K}_{\text{ii}} \end{bmatrix} \tag{9}$$

where subscript i denotes inflow nodes and subscript o denotes non-inflow nodes. Minimising energy with respect to non-inflow nodes whilst treating inflow as prescribed yields:

$$\boldsymbol{h}_{\text{oth}} = -\boldsymbol{K}_{\text{oo}}^{-1}\boldsymbol{K}_{\text{oi}}\boldsymbol{h}_{\text{in}} \equiv \boldsymbol{K}_{\text{oth}}\boldsymbol{h}_{\text{in}} \tag{10}$$

A relation matrix $\boldsymbol{C}$ compactly expresses the complete field as a linear function of inflow values:

$$\boldsymbol{h} = \boldsymbol{C} \cdot \boldsymbol{h}_{\text{in}} \tag{11}$$

Optimal inflow thickness is obtained by minimising total material volume:

$$\min_{\boldsymbol{h}_{\text{in}}} \frac{1}{2}\boldsymbol{h}_{\text{in}}^T(\boldsymbol{C}^T\boldsymbol{M}\boldsymbol{C})\boldsymbol{h}_{\text{in}} + (\boldsymbol{C}^T\boldsymbol{M}\boldsymbol{u})^T\boldsymbol{h}_{\text{in}} \tag{12}$$

where $\boldsymbol{M}$ is the lumped mass matrix ($M_{ii} = \sum_e A_e/3$) and $\boldsymbol{u}$ a vector of ones. The quadratic term represents total material volume whilst the linear term prevents trivial solutions. The complete field is then recovered and normalised:

$$\boldsymbol{H} = \frac{\boldsymbol{h}}{\min(\boldsymbol{h})} \tag{13}$$

The resulting distribution minimises material volume subject to smooth variation transverse to fibre directions. It represents material accumulation as fibres pass from inflow to outflow boundaries.

2.3. Stream Function Computation

The fibre-aligned reference frames $[\tilde{\boldsymbol{p}}_i, \tilde{\boldsymbol{q}}_i]$ and the normalised thickness field $\boldsymbol{H}$ together define a thickness-weighted vector field over the mesh. This field is formally analogous to an incompressible flow field: material enters at inflow boundaries, traverses the surface without crossing adjacent tow paths, and exits at outflow boundaries. A scalar stream function ψ is therefore defined over the mesh such that its iso-contours are everywhere tangent to the thickness-weighted fibre directions, yielding the course centrelines.

The stream function is obtained by solving a Laplacian system $\boldsymbol{L}\boldsymbol{\psi} = \boldsymbol{f}_s$, where $\boldsymbol{L}$ is the mesh Laplacian matrix (the same matrix assembled in Section 2.1) and the source term $\boldsymbol{f}_s$ is assembled from the thickness-weighted fibre directions. For each triangular element, a representative flow direction is computed as the thickness-weighted average of the nodal fibre directions $\tilde{\boldsymbol{p}}_i$ (defined in Equation 7):

$$\boldsymbol{v} = -\frac{1}{3}(H_1\tilde{\boldsymbol{p}}_1 + H_2\tilde{\boldsymbol{p}}_2 + H_3\tilde{\boldsymbol{p}}_3) \tag{14}$$

The negative sign ensures alignment with material flow from inflow to outflow. Projecting this flow vector onto the element edge vectors $\boldsymbol{l}_i$ yields local contributions to the source term:

$$f_{s,i}^{(e)} = \frac{1}{2}\boldsymbol{v}^{(e)} \cdot \boldsymbol{l}_i \quad \text{for } i = 1, 2, 3 \tag{15}$$

To ensure uniqueness, one nodal value is fixed (removing the Laplacian's null space). The solution is then shifted to ensure non-negativity:

$$\boldsymbol{\psi}^* = \boldsymbol{\psi} - \min(\boldsymbol{\psi}) \tag{16}$$

The resulting stream function field provides iso-contours that define smooth, manufacturable fibre paths that respect the given fibre angle distributions. The resultant stream function field is presented in Figure 5.

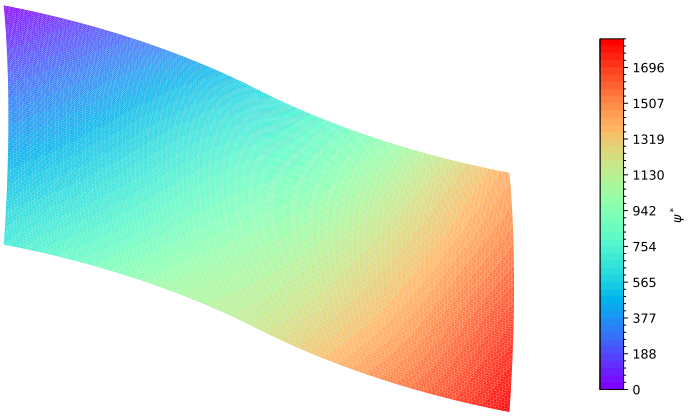

Figure 5: Contour map of the resultant stream function field

2.4. Course Path Extraction

The iso-contours of the stream function ψ define candidate fibre trajectories across the surface. The task now is to select a subset of these contours as course centrelines, spaced to satisfy manufacturing constraints. Two requirements govern the placement:

1. **Minimum spacing:** Adjacent course centrelines must be separated by at least one tow width w to prevent overlaps. Overlapping courses produce local thickness build-ups that compromise bonding quality and introduce surface discontinuities detrimental to aerodynamic performance.
2. **Path continuity:** Gaps between adjacent courses, whilst undesirable, are tolerated as a design concession. Although gaps and overlaps could in principle be minimised by dropping and restarting tows mid-course, doing so interrupts the intended load path. Consequently, course continuity is prioritised over gap elimination.

The stream function provides a simple mechanism for course placement: a course path at any location is obtained by extracting the iso-contour at the local ψ value. The complete extraction procedure operates as follows:

1. **Initialisation:** The initial course is placed at the median stream value ψ_{med} and the corresponding iso-contour is extracted. Subsequent courses are generated bidirectionally from this seed, sweeping in the direction of increasing ψ and decreasing ψ, until the surface boundary is reached. The most recently generated course serves as the reference for the subsequent offset computation.
2. **Geodesic offset:** For each reference course, points along the centreline are offset by one tow width w in the $\tilde{\boldsymbol{q}}$-direction. Since the surface exhibits non-zero Gaussian curvature, Euclidean offsets do not represent the true on-surface spacing; a geodesic offset computed via a walk-and-project approach on the triangulated mesh is used instead. While this approach introduces small geometric inaccuracies, it avoids the computational cost of surface parametrisation and provides a practical approximation of the true geodesic offset.
   At each point $\boldsymbol{c}_i$ along the reference course, the fibre-aligned frame vector $\tilde{\boldsymbol{q}}_i$ (from Equation 7) defines the offset direction, lying in the tangent plane by construction ($\tilde{\boldsymbol{q}}_i = \boldsymbol{N}_i \times \tilde{\boldsymbol{p}}_i$). Starting from $\boldsymbol{x}_0 = \boldsymbol{c}_i$, each step displaces the current point along the tangent-corrected direction. Since $\tilde{\boldsymbol{q}}$ is interpolated from mesh nodes rather than recomputed at each walking point, a correction is first applied at each step to project it onto the local tangent plane:

$$\tilde{\boldsymbol{q}}^* = \frac{\tilde{\boldsymbol{q}} - (\tilde{\boldsymbol{q}} \cdot \boldsymbol{N}_k)\boldsymbol{N}_k}{\|\tilde{\boldsymbol{q}} - (\tilde{\boldsymbol{q}} \cdot \boldsymbol{N}_k)\boldsymbol{N}_k\|} \tag{17}$$

   where $\boldsymbol{N}_k$ is the surface normal at walking step k. The point is then displaced by Δs along $\tilde{\boldsymbol{q}}^*$ and projected back onto the mesh via the surface projection operator $\Pi(\cdot)$:

$$\boldsymbol{x}_{k+1} = \Pi(\boldsymbol{x}_k + \Delta s\, \tilde{\boldsymbol{q}}^*) \tag{18}$$

   The surface distance traversed is accumulated as:

$$d_{k+1} = d_k + \|\boldsymbol{x}_{k+1} - \boldsymbol{x}_k\| \tag{19}$$

   The walk terminates when $d \geq w$, yielding the offset point $\boldsymbol{o}_i = \boldsymbol{x}_{k+1}$. As $\Delta s \to 0$, the accumulated distance d converges to the true geodesic distance. The resulting set of offset points $\{\boldsymbol{o}_i\}$ then define the offset course.
3. **Course selection:** The stream function value ψ is interpolated at each offset point $\boldsymbol{o}_i$, and the next-course stream value is selected as:

$$\psi_{\text{next}} = \begin{cases} \min\left(\psi(\boldsymbol{o}_i)\right) & \text{traversing in direction of increasing } \psi \\ \max\left(\psi(\boldsymbol{o}_i)\right) & \text{traversing in direction of decreasing } \psi \end{cases} \tag{20}$$

   Taking the extremum ensures the resulting iso-contour is displaced by *at least* one tow width from the reference course, favouring overlap-free deposition in accordance with the minimum spacing requirement above. A less conservative selection, such as taking the mean offset ψ value, would reduce gaps at the expense of introducing some overlaps, representing an alternative design choice. Furthermore, by taking the iso-contour of a stream function value, the resultant course closely aligns with the defined fibre angles. The resultant offset course then becomes the reference course for the subsequent iteration.

4. **Termination:** The process repeats until: (i) all projected offset points fall outside the surface projection tolerance, indicating the offset has exited the mesh domain; or (ii) $|\psi_{\text{next}} - \psi_{\text{prev}}| < \varepsilon$, indicating that the stream function is no longer advancing meaningfully between iterations. The procedure runs independently in both sweep directions, and the resulting courses are combined into the final set.

The complete course extraction procedure, including the geodesic walk subroutine, is summarised in Figure 6.

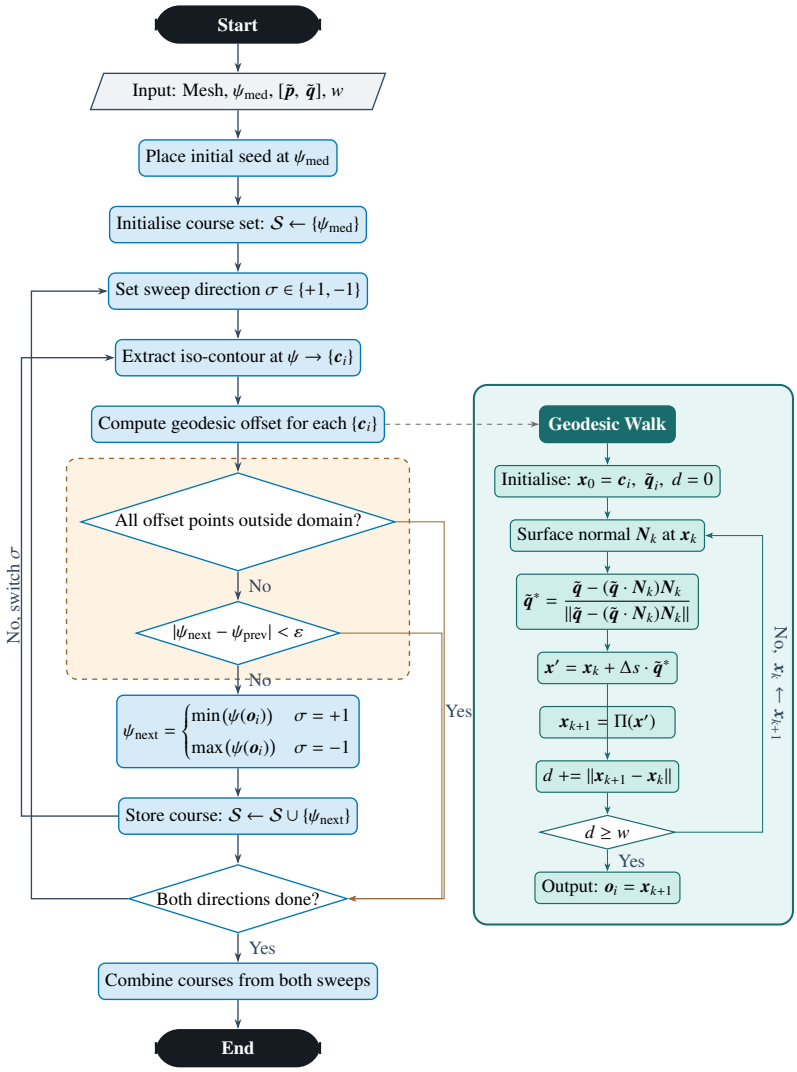

Figure 6: Course extraction algorithm with geodesic walk subroutine

3. Results

The standard AFP tow width corresponds to one quarter of an inch (6.35 mm). Course centrelines were extracted at this spacing as described in Section 2, and tow edges were obtained by offsetting the centrelines by half the tow width w in the transverse direction (equation 21). The resultant tow layout is visualised in Figure 7.

$$\boldsymbol{x}_{\text{edge}} = \boldsymbol{x}_{\text{centre}} \pm \frac{w}{2}\,\tilde{\boldsymbol{q}} \tag{21}$$

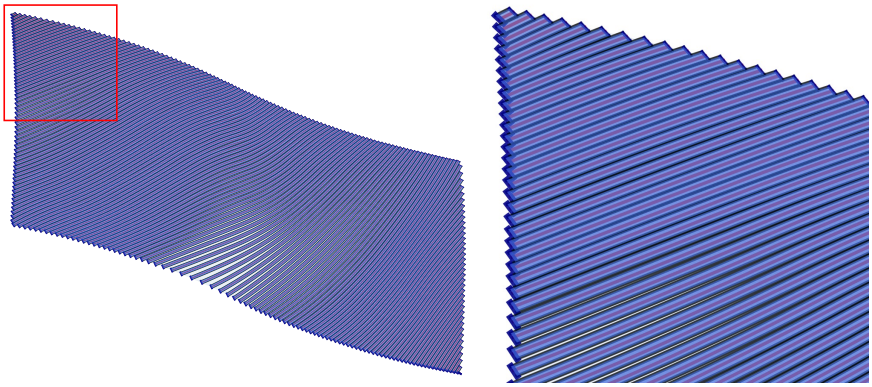

Figure 7: Resultant tows on the test geometry (right: zoomed view of red region).

The resultant fibre angle deviations are presented in Figure 8. The deviation at each course point is computed by comparing the course tangent angle, derived from the extracted course centreline, against the prescribed fibre angle interpolated from the nodal fibre angle distribution to that location. The maximum positive deviation of +5.06° occurs at Course 134, where the prescribed angle is 58.18° and the computed angle is 63.25°. The maximum negative deviation of −3.98° occurs at Course 39, where the prescribed angle is 41.03° and the computed angle is 37.06°. The largest deviations occur near the edges of the geometry.

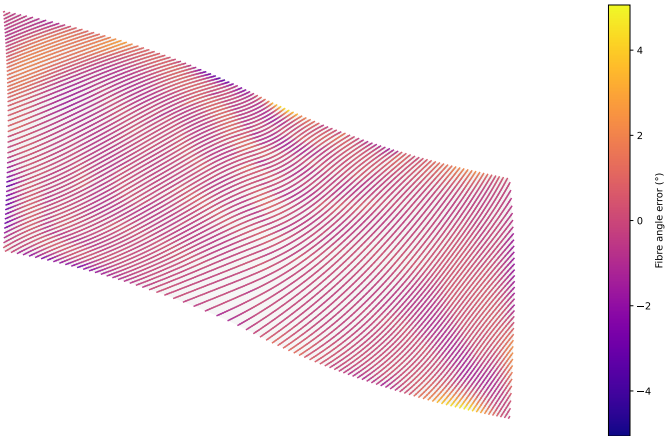

Figure 8: Fibre angle deviations across the course centrelines

To check for potential overlaps, the minimum geodesic distance between adjacent courses was computed sequentially from the top-left to the bottom-right course. The closest pair (interface 41) has a minimum spacing of 6.19 mm, a 2.5% undershoot relative to the

nominal width. The results suggest that overlaps are largely avoided across the laminate, except in a few cases. It must be noted, however, that the *pygeodesic* library in Python was used to compute the geodesic spacing between adjacent tows, and the results show high mesh dependency. To the best of the authors' knowledge, no better alternative is available for this computation in the present context and the results are therefore presented as obtained. This may account for the variation observed in Figure 9. Visual inspection of Figure 7 suggests that courses are placed as intended, with no visible overlaps, though gaps cannot be excluded.

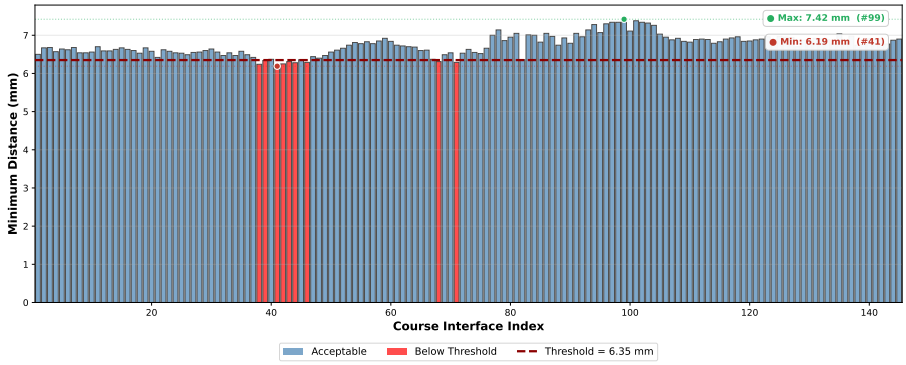

Figure 9: Minimum geodesic distance between adjacent courses

4. Conclusion

This work demonstrates that the streamline analogy, previously used for planar geometries, extends effectively to doubly-curved surfaces. Computing the stream function directly on the discretised surface and applying a geodesic walk-and-project offset together enable course extraction at intended spacing.

Evaluation on a Gaussian-curvature geometry at the standard AFP tow width of 6.35 mm showed that the extracted courses closely follow the prescribed fibre angle distribution, with deviations remaining within $-3.98°$ and $+5.06°$ across the laminate. Whilst fibre angle deviation provides a direct measure of path fidelity, comparing the stiffness distribution of the resulting laminate against the designed distribution would offer a more meaningful assessment, as it directly reflects the structural consequence of any deviation. Since the present study employs a synthetic fibre angle distribution rather than one derived from a structural optimisation, such a comparison was not carried out here, and is instead recommended as a direction for future work.

Inter-course spacing was maintained within 2.5% of the nominal tow width, although this should be interpreted with caution. Together with visual inspection of the courses, these results indicate that the geodesic offset strategy prevents overlaps across the laminate, though the reliability of the quantitative spacing analysis remains limited by the mesh dependency of the *pygeodesic* library.

5. Acknowledgements

This research was supported by the Dutch government programme 'Luchtvaart in Transitie'.

6. References

[1] Adriana W Blom, Mostafa M Abdalla and Zafer Gürdal. "Optimization of course locations in fiber-placed panels for general fiber angle distributions". In: *Composites Science and Technology* 70.4 (2010), pp. 564–570.

[2] Zafer Guerdal and Reynaldo Olmedo. "Composite laminates with spatially varying fiber orientations-'Variable stiffness panel concept'". In: *33rd structures, structural dynamics and materials conference*. 1992, p. 2472.

[3] M. Hijne. "A Fibre-Path Generation Algorithm for Fibre-Steered Variable Stiffness Laminates". Faculty of Aerospace Engineering. Master's Thesis. Delft University of Technology, July 2022.

[4] Samuel Tsunduka IJsselmuiden. "Optimal design of variable stiffness composite structures using lamination parameters". In: *Delft University of Technology* (2011), pp. 1–210.

[5] G Gonzalez Lozano, A Tiwari and C Turner. "A design algorithm to model fibre paths for manufacturing of structurally optimised composite laminates". In: *Composite Structures* 204 (2018), pp. 882–895.

[6] Daniël MJ Peeters, Gustavo Gonzalez Lozano and Mostafa M Abdalla. "Effect of steering limit constraints on the performance of variable stiffness laminates". In: *Computers & Structures* 196 (2018), pp. 94–111.

[7] Caleb R Pupo et al. "Retrieving tow paths from a fiber angle distribution on single, and double curved surfaces". In: *AIAA Scitech 2019 Forum*. 2019, p. 0421.

[8] Guillaume Rousseau et al. "Automated Fiber Placement Path Planning: A state-of-the-art review." In: *Computer-Aided Design & Applications* 16.2 (2019).